








A Comprehensive Analysis of Attenuation Characteristics Using Strong Ground Motion Records for the Central Seismic Gap Himalayan Region, India

Himanshu Mittal ^a, Babita Sharma ^b, Wei-an Chao ^c, Yih-Min Wu ^{a,d,e}, Ting-Li Lin ^f, and Prasanta Chingtham^b

^aDepartment of Geosciences, National Taiwan University, Taipei, Taiwan; ^bNational Centre for Seismology, Ministry of Earth Sciences, New Delhi, India; ^cCivil Engineering Department, National Chiao Tung University, Hsinchu, Taiwan; ^dNTU Research Center for Future Earth, National Taiwan University, Taipei, Taiwan; ^eInstitute of Earth Sciences, Academia Sinica, Taipei, Taiwan; ^fDepartment of Earth Sciences, National Cheng Kung University, Tainan, Taiwan

ABSTRACT

This study aims to estimate attenuation characteristics of the central Himalayan region of India concerning various strong-motion parameters such as Kappa value (κ) and site effects. We have tried to elaborate on the regional structural heterogeneities and their implications towards the seismic hazard assessment of the study region. A total of 81 earthquakes recorded at 50 stations situated in the central Himalayan region of India are used for the purpose. The particular focus is kept on Kappa value, which shows variability from 0.03 s to 0.095 s, inferring the higher values obtained in plains with deep sediment accumulations proving high-frequency energy dissipation and stiff-soil/rocky sites exhibit comparatively limited attenuation accordingly. To substantiate these results various attenuation parameters such as coda wave quality factor (Q_c), intrinsic attenuation parameter (Q_i), and scattering attenuation parameter (Q_s), have been estimated for two regions in the central seismic gap Himalayan region of India employing the single backscattering model and Wennerberg formulation. The estimated values of Q_c , Q_i , and Q_s are found to be highly dependent on frequency in the frequency range 1.5–24 Hz for both the regions. The average frequency-dependent relationships ($Q = Q_0 f^\eta$) estimated for both regions are $Q_c = 158f^{1.18}$ and $Q_c = 194f^{1.2}$, respectively. The low value of Q_0 shows that the region is highly heterogeneous while the higher value of η indicates higher seismicity in the area. It is also found that intrinsic attenuation is predominant over the scattering attenuation, envisaging the behavior of the wave attenuation through the absorption within the granitic layer at shallow depths. At lower frequencies, Q_c values are found close to Q_s values, which is in agreement with the theoretical measurements suggesting the presence of complex crustal heterogeneities beneath the region affecting the propagation of seismic waves experiencing considerable decay of energy through scattering. To confirm the aggregate attenuation on the stations, the site characteristics are also determined for examining the behavior of the amplification as the ground motion is comprised of the combined effect of the source, path, and site. The sites are amplified at a predominant frequency (f_{peak}) in between 1.5 to 10 Hz for the central Himalayan region. The different attenuation and amplification parameters like kappa, Q , and site effects can be utilized for detailed seismic hazard analysis (based on ground motion prediction equations) of the area as this region is of great importance from a socio-economic point of view.

ARTICLE HISTORY

Received 6 September 2019
Accepted 11 May 2020

KEYWORDS

Kappa value (κ); quality factor (Q_c); Central Himalayan region; predominant frequency (f_{peak})

CONTACT Himanshu Mittal  himanshumitt10@gmail.com  Department of Geosciences, National Taiwan University, Taipei, Taiwan

1. Introduction

The Himalayan region in India is regarded as one of the most seismically active areas in the world. Considering the seismic zoning map of India, most of the part of Indian Himalayan belt falls in Zone IV and V (the two most severe zones on a scale of II to V, Bureau of Indian Standards (BIS) 2002). India faces seismic activity mainly from three regions: Himalayan belt in North West (NW) and North East (NE) India, Gujarat in Western India, and Andaman and Nicobar in the southeast part of India. Out of these three areas, the Himalayan belt has witnessed great and significant earthquakes in the past. Broadly, the entire Himalayan belt can be divided into three seismic gaps where some great earthquake did not erupt in the last centuries and maybe the future locale of some bigger earthquake (Khattri 1987). These gaps are the Kashmir gap (extending to the NW side of the 1905 Kangra earthquake), central seismic gap (lying between the epicenter of the 1905 Kangra earthquake and 1934 Bihar-Nepal earthquake), and NE gap extending towards the NE side of 1934 Nepal Bihar earthquake (Fig. 1). Some moderate to bigger earthquakes are witnessed in the Kashmir gap (e. g. Muzaffarabad earthquake of 2005) and NE gap in recent times; while no significant earthquake occurred in the central seismic gap (CSG). The probability of occurrence of any considerable earthquake in CSG in the coming 80 years is estimated to be 0.59 (Khattri 1999). Some of the earthquakes occurred in CSG in 1803 and 1833, but these were not gap filling. One of the major earthquake (M_w 7.9) occurred in 2015 in Nepal but this earthquake also occurred outside CSG and thus accumulated stresses in this area may be responsible for the future bigger earthquake. Though, the recent Nepal

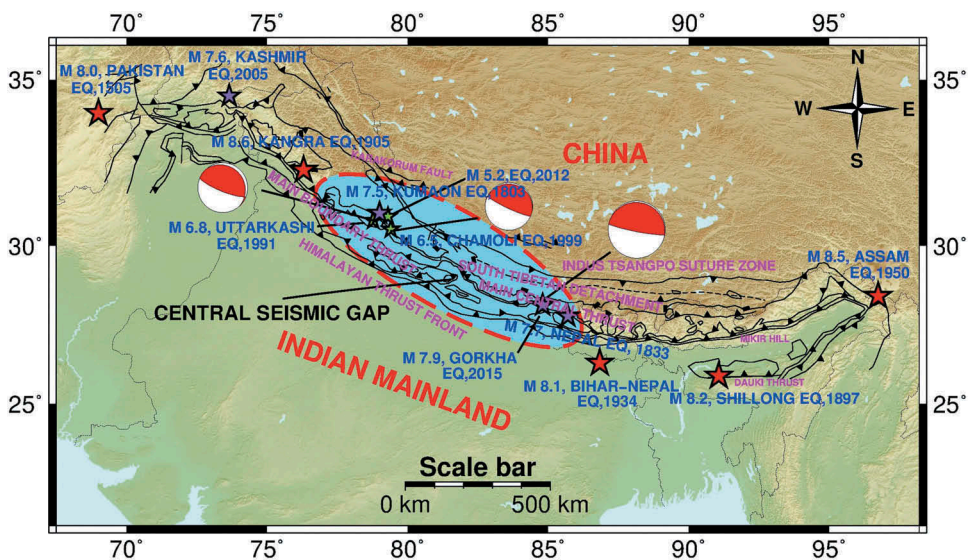


Figure 1. Seismotectonic map showing different prominent structural features in the Himalayan region under study area. Important Himalayan tectonic features like Main Boundary Thrust (MBT), Main Central Thrust (MCT), Main Frontal Thrust (MFT) are plotted along with other features like Indus Tsangpo Suture Zone (ITSZ) and South Tibetan Detachment (STD). The location of various historical earthquakes is shown. Earthquakes of different magnitude ranges are shown in different colors. Central seismic gap, the location of the future possible earthquake is also marked.

earthquake of 2015 was far away from the Indian region, it still caused considerable losses in Indian states like Uttar Pradesh and Bihar, around 250 Km away from the epicenter. Given the importance of urbanization and industries in the area, any bigger earthquake in CSG will cause huge damage to human life as well as man-made structures. In view of this, a reliable estimation of seismic hazard in this area is required. The seismic hazard of an area is based on the ground motion prediction equations (GMPEs) employing strong ground motion data available from previously recorded earthquakes. India is one of the countries, where very few strong motion data is available prior to 2005. At that time, GMPEs were developed using synthetic data or using the strong motion data from regions having the same conditions. However, for accurate hazard prediction, all the input parameters like the site, source, and path should be site and region specific. Region-specific GMPEs are the statistical models to estimate various shaking parameters like peak ground acceleration (PGA) and response spectra, as a function of source, site and path parameters. The observed ground motion at a site is a combined function of source, site, and path for each earthquake. Various researchers have studied attenuation of seismic waves from the source to the recording site in the last decade (Aki and Richards 2002). In spite of the same magnitude for many earthquakes, different values of shaking parameters like PGA, peak ground velocity (PGV), and spectral acceleration (SA) may be observed at a site. The simple reason for this difference in shaking parameters may be due to path and site effects which may change its frequency and amplitude content and cause above mentioned difference in the recordings. Seismic waves traveling from the source to the recording site get amplified or attenuated. Amplification may be attributed to the site conditions while, attenuation is a function of path effect. Attenuation of seismic waves may be referred to as decay in amplitude with distance consisting of all three factors; source, site, and path. A few studies have been carried out in this region keeping in mind the attenuation as well as amplification (Kumar, Ram, and Khattri 2006; Nath, Shukla, and Vyas 2008; Sharma, Chopra, and Roy 2014; Sharma et al. 2009; Singh et al. 2002). All these studies address to attenuation by considering the Q value, which represents the total attenuation. There is another factor called kappa (κ), which plays a significant role in the high – frequency decay of the spectrum (Anderson and Hough 1984). Very few studies are available regarding κ in the Himalayan region, which may be an important parameter in strong motion simulation as well as GMPEs. Sharma, Chopra, and Roy (2014) estimated κ -value in central Himalayas using few recorded earthquakes and clearly lacks processing in terms of κ value. They showed that average κ -value varies between 0.023 s to 0.07 s at different sites. The fewer studies relating to κ -value in the central Himalayas motivated us to study the attenuation and amplification characteristics of central Himalayas with the special emphasis on κ and its dependence on the source, site, and path parameters.

2. Study Area & Seismic Data

The Himalayas are formed by the convergence of the northward-driving Indian plate that continues to dip under the Eurasian plate. High ongoing tectonic activity due to these convergences has given rise to many fault systems in the region. Some of the most prominent features in the area include the Indian–Tsangpo collision suture zone (ISZ),

Main Boundary Thrust (MBT), the Main Central Thrust (MCT), and the Main Frontal Thrust (MFT) (Fig. 1). In addition to the aforementioned main features, many small folds, faults, and lineaments like Munsiri Thrust (MT), the Vaikrita Thrust (VT), Jawalamukhi thrust (JMT), Sundernagar fault (SuF), Kistwar fault (KF) and Drang Fault (DF) exist in the region.

In general, the seismicity in the central Himalayas is of the interplate type where most of the earthquakes are centered on MCT, the central part of the east-west extended Himalayan mountain zone (Seeber and Armbruster 1981). This main Himalayan seismic belt around MCT is extended towards MBT, and the seismicity between MBT and MCT is linked to reactivation of the parallel low angle detachment thrust faults in the upper crust (Khattari et al. 1989). The available focal mechanism in the central Himalayas suggests that the tectonic features are marked as thrust dipping toward the northeast (Gahalaut and Rao 2009). The focal mechanism of some prominent earthquakes in the region like the Uttarkashi earthquake of 1991, the Chamoli earthquake of 1999, and the most recent Gorkha earthquake of 2015 support this mechanism of thrust dipping. Most of the earthquakes occur at shallow depths, generally in the upper 20 km (Gaur et al. 1985), which are responsible for high destruction.

All the earthquakes used in present work are recorded by the strong motion instrumentation network installed by the Indian Institute of Technology, Roorkee (IITR) under a project funded by the Ministry of Earth Science, New Delhi (MoES). This instrumentation consisting of 300 instruments was installed in seismic zone IV and V in the Himalayan belt, as well as, some of the thickly populated cities falling in zone III. All of these instruments have a wide dynamic range (108 dB), to provide precise records in the near field (Kumar and Mittal 2018; Mittal et al. 2006). The instruments are equipped with external GPS for time correction. This instrumentation started in November 2005 and just after one month of installation, the first moderate earthquake having M 5.2 was recorded by this network at eight stations in the Uttarakhand Himalayas in CSG. The location of this earthquake was close to historical Chamoli earthquake of 1999 (M_w 6.5), which caused widespread damage in the area. After that, a lot of earthquakes, originating in the Himalayan belt, were witnessed by this network and recorded data has been used in various studies (e. g. Kumar, Kumar, and Mittal 2013; Kumar et al. 2017; Mittal et al. 2019a, 2018).

In the present study, the strong motion data of 81 events recorded in the period from 2005 to 2014 in Himachal and Uttarakhand Himalayan belt has been used (Fig. 2). The earthquake information like location, origin time, date, and the number of recorded stations are summarized in Table 1. In total, 50 strong-motion sites as per Table 2, situated in Himachal Pradesh and Uttarakhand states are used in present work. Though data for smaller earthquakes is available at some more locations other than these used 50 sites in the present study, we avoid them as data is available only at one place and their magnitude is not reported by the reporting agency, which is Indian Meteorological Department (IMD) in our case. Complete detail of used stations along with available information is available in Table 2.

3. Kappa Value

The decay of the amplitude spectra with frequency is characterized by high-frequency decay parameter kappa (κ). Lower κ values correspond to higher ground motion, while

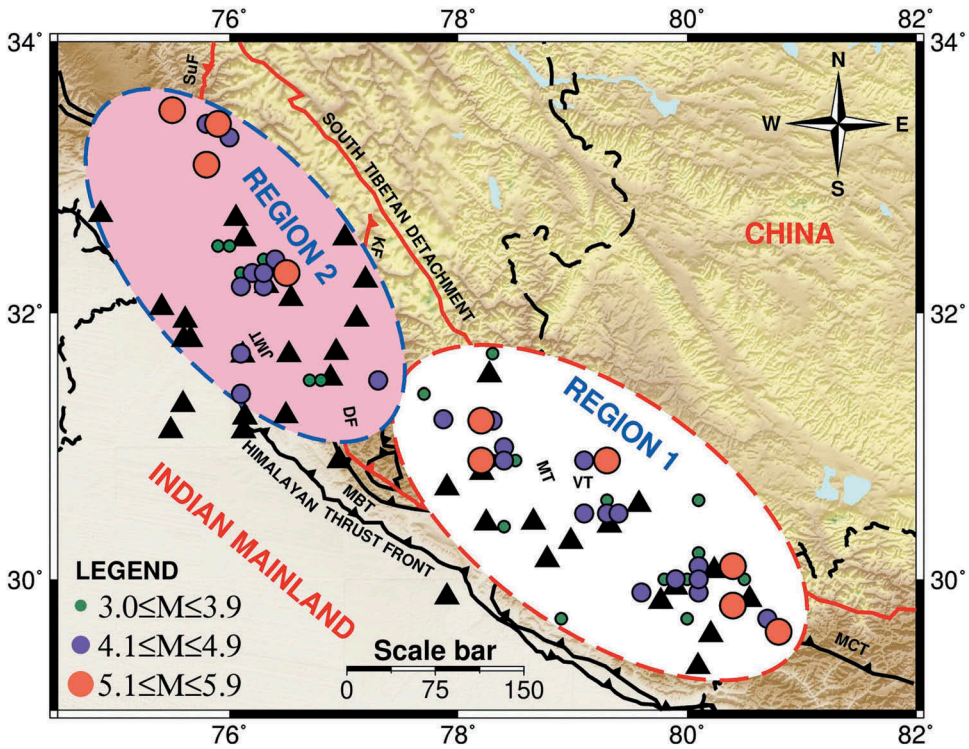


Figure 2. The map showing the location of recording stations as well as earthquakes used in the present analysis. The different earthquakes used in the present study are plotted according to size. Various regional features like Munsiri Thrust (MT), the Vaikrita Thrust (VT), Jawalamukhi thrust (JMT), Sundernagar fault, Kistwar fault (KF) and Drang Fault have plotted along with major faults like Main Boundary Thrust (MBT) and Min Central Thrust (MCT). The stations recording these earthquakes are shown as triangles. The two regions used for Q estimation are shown as region 1 with a red outline and 2 with blue outline respectively. The earthquake data is collected from <https://pesmos.com/> (Kumar and Mittal 2018).

higher values imply lower ground motion (Mena et al. 2010). κ values play an important role in GMPE. In addition to GMPE, κ is also important in stochastic ground-motion simulation methods to limit the attenuation, and the spectral shape of the synthetic seismogram. A number of techniques are available in the literature to estimate κ values. These involve the use of acceleration spectra (Anderson and Hough 1984; Lai et al. 2016), displacement spectra (Biasi and Smith 2001; Perron et al. 2017), and response spectra (Silva and Darragh 1995). In the classic method introduced by Anderson and Hough (1984), κ value is estimated from the linear range of acceleration spectra well above the corner frequency having a sufficient signal-to-noise (SNR) ratio. This method is beneficial for the earthquakes having a magnitude > 3.5 . Anderson and Humphrey (1991) applied this standard approach of estimating the κ value to lower magnitude earthquakes by considering κ to be the slope of residuals. In the low seismicity regions, separation of corner frequency from the κ effect becomes difficult. In order to overcome this problem, Biasi and Smith (2001) introduced the use of low frequency displacement spectra. Though κ is an important parameter in different applications like strong ground simulation (e. g. Boore 2003; Mittal and Kumar 2015; Mittal, Kumar, and Kamal 2013;

Table 1. Table showing the details of used earthquakes in the present study.

S. No	Year	Month	Date	Latitude (°N)	Longitude (°E)	Depth (km)	Magnitude	Agency
1	2005	12	14	30.9	79.3	26	5.2	IMD
2	2006	12	10	31.5	76.7	33	3.5	IMD
3	2007	07	22	31.2	78.2	33	5.0	IMD
4	2007	10	04	32.5	76.0	10	3.8	IMD
5	2008	08	19	30.1	80.1	15	4.3	IMD
6	2008	09	04	30.1	80.4	10	5.1	IMD
7	2008	10	21	31.5	77.3	10	4.5	IMD
8	2009	01	03	36.5	70.8	188	6.4	IMD
9	2009	01	09	31.7	78.3	16	3.8	IMD
10	2009	01	31	32.5	75.9	10	3.7	IMD
11	2009	02	25	30.6	79.3	10	3.7	IMD
12	2009	03	18	30.9	78.2	10	3.3	IMD
13	2009	05	15	30.5	79.3	15	4.1	IMD
14	2009	07	17	32.3	76.1	10	3.7	IMD
15	2009	08	27	30.0	80.0	14	3.9	IMD
16	2009	09	21	30.9	79.1	13	4.7	IMD
17	2009	10	03	30.0	79.9	15	4.3	IMD
18	2009	10	22	36.5	71.0	168	6.3	IMD
19	2009	10	29	27.3	91.4	5	5.2	IMD
20	2009	12	06	35.8	77.3	60	5.3	IMD
21	2010	01	11	29.7	80.0	15	3.9	IMD
22	2010	02	22	30.0	80.1	2	4.7	IMD
23	2010	03	14	31.7	76.1	29	4.6	IMD
24	2010	05	01	29.9	80.1	10	4.6	IMD
25	2010	05	03	30.4	78.4	8	3.5	IMD
26	2010	05	28	31.2	77.9	43	4.8	IMD
27	2010	05	31	30.0	79.8	10	3.6	IMD
28	2010	07	06	29.8	80.4	10	5.1	IMD
29	2010	07	10	29.9	79.6	10	4.1	IMD
30	2010	08	13	31.4	77.7	6	3.4	IMD
31	2010	09	17	36.5	70.8	167	6.5	IMD
32	2011	03	14	30.5	79.1	8	3.3	IMD
33	2011	03	21	36.5	70.9	166	5.7	IMD
34	2011	04	04	29.6	80.8	10	5.7	IMD
35	2011	05	04	30.2	80.4	10	5.0	IMD
36	2011	06	15	30.6	80.1	10	3.4	IMD
37	2011	06	20	30.5	79.4	12	4.6	IMD
38	2011	06	23	30.0	80.5	5	3.2	IMD
39	2011	07	28	33.3	76.0	21	4.4	IMD
40	2011	09	21	30.9	78.3	10	3.1	IMD
41	2011	09	24	30.9	78.3	10	3.0	IMD
42	2011	10	26	31.5	76.8	5	3.5	IMD
43	2012	01	16	29.7	78.9	10	3.6	IMD
44	2012	02	09	30.9	78.2	10	5.0	IMD
45	2012	02	26	29.6	80.8	10	4.3	IMD
46	2012	05	10	30.2	79.4	5	3.9	IMD
47	2012	07	12	36.5	70.9	170	6.3	IMD
48	2012	07	28	29.7	80.7	10	4.5	IMD
49	2012	08	13	34.8	73.7	30	5.2	IMD
50	2012	08	23	24.8	82.7	10	5.0	IMD
51	2012	10	02	32.4	76.4	10	4.5	IMD
52	2012	10	02	32.3	76.3	10	4.9	IMD
53	2012	10	03	32.4	76.3	5	3.8	IMD
54	2012	10	03	32.4	76.3	10	3.6	IMD
55	2012	10	03	32.4	76.3	10	3.4	IMD
56	2012	11	06	32.3	76.2	5	4.1	IMD
57	2012	11	11	29.2	81.5	10	5.0	IMD
58	2012	11	11	32.3	76.2	5	4.0	IMD
59	2012	11	15	30.2	80.1	5	3.0	IMD
60	2012	11	27	30.9	78.4	12	4.8	IMD
61	2013	01	02	29.4	81.1	10	4.8	IMD

(Continued)

Table 1. (Continued).

S. No	Year	Month	Date	Latitude (°N)	Longitude (°E)	Depth (km)	Magnitude	Agency
62	2013	01	09	29.8	81.7	34	5.0	IMD
63	2013	01	10	30.1	80.4	5	3.2	IMD
64	2013	01	29	30.0	81.6	7	4.0	IMD
65	2013	02	11	31.0	78.4	5	4.3	IMD
66	2013	02	17	30.9	78.4	10	3.2	IMD
67	2013	04	06	30.5	79.1	10	4.3	IMD
68	2013	05	01	33.1	75.8	15	5.8	IMD
69	2013	05	14	33.4	75.8	10	4.8	IMD
70	2013	06	04	32.7	76.7	10	4.8	IMD
71	2013	07	09	32.9	78.4	10	5.1	IMD
72	2013	07	13	32.2	76.3	10	4.5	IMD
73	2013	08	02	33.5	75.5	28	5.4	IMD
74	2013	08	02	33.4	75.9	20	5.2	IMD
75	2013	08	29	31.4	76.1	10	4.7	IMD
76	2013	09	05	30.9	78.5	11	3.5	IMD
77	2013	10	20	35.8	77.5	80	5.5	IMD
78	2013	11	06	31.4	76.1	10	4.9	IMD
79	2013	12	25	31.2	78.3	10	4.0	IMD
80	2014	06	17	32.2	76.1	10	4.1	IMD
81	2014	08	21	32.3	76.5	10	5.0	IMD

Mittal et al. 2016b, 2019b; Motazedian and Atkinson 2005) and GMPEs, its origin, and relation to different parameters is highly questionable. Many studies have been performed around the world to estimate κ values. Most of the previous studies have considered kappa to be a site-specific parameter (Anderson and Hough 1984; Hanks 1982), while some other studies find κ to depend on source, path or a combination of two or all three factors (Papageorgiou and Aki 1983; Purvance and Anderson 2003; Tsai and Chen 2000). In general, most of the studies have addressed κ value to be related to site and path effects (e. g. Fernández, Castro, and Huerta 2010; Hough and Anderson 1988; Ktenidou, Gélis, and Bonilla 2013; Ktenidou et al. 2017; van Houtte et al. 2014).

The primary method introduced by Anderson and Hough (1984) is one of the most widely used methods. As proposed by Anderson and Hough (1984), κ can be represented exponentially by the following relation:

$$A(f) = A_0 \exp(-\pi \kappa f), \quad f_1 < f < f_2 \quad (1)$$

Where f_1 and f_2 are the lowest and highest frequencies between which the decay of the Fourier amplitude spectrum is linear.

Following relation is used to estimate κ values from the slope of the acceleration amplitude spectrum using least square fitting method:

$$\kappa = -\lambda/\pi, \quad \lambda = \Delta(\ln a)/\Delta f \quad (2)$$

where Δf is the frequency range defined by $\Delta f = f_2 - f_1$, a is acceleration spectrum, and λ is the slope.

κ value is one of the most critical parameters in the stochastic simulation in the area, where too much ground motion recordings are not available.

κ can be separated in the source, site, and path terms as follows:

$$\kappa = \kappa_0 + \kappa_s + \kappa(R) \quad (3)$$

Table 2. Estimated kappa values, predominant frequency, amplification at the predominant frequency, and the number of records used for estimating kappa at different sites under study.

Station	Station Code	Predominant Frequency f_{peak} (Hz)	Amplification (A_{max})	Average Kappa κ (s)	Number of Records for κ estimation
Amb	AMB	2.70	7.92	0.0707	1
Almora	ALM	2.00	3.97	0.0543	2
Bageshwar	BAG	1.60	5.26	0.0472	6
Barkot	BAR	3.11	5.44	0.0499	8
Bilaspur	BIL	1.00	4.27	0.0712	1
Chakrata	CKR	1.60	4.91	0.0531	4
Chamba	CHM	2.10	3.70	0.0543	17
Chamoli	CHA	1.40	10.20	0.0571	7
Champawat	CHP	5.79	6.50	0.0524	5
Dehra	DEH	7.40	3.37	0.0418	2
Dehradun	DHR	2.73	5.17	0.0679	2
Dhanaulti	DNL	1.60	15.32	0.0615	5
Dharamshala	DSL	2.34	5.55	0.0346	2
Dharchula	DRC	1.83	5.17	0.0324	4
Didihat	DDH	10.50	2.78	0.0364	1
Garsain	GAR	2.29	4.42	0.0478	5
Ghanshali	GHA	3.56	5.03	0.0557	2
Hamirpur	HAM	2.96	5.85	0.0846	3
Jammu	JMU	1.34	6.94	0.0446	3
Joshimath	JSH	1.53	2.71	0.0582	2
Jubbal	JUB	5.54	3.49	0.0235	2
Kapkot	KAP	3.72	8.89	0.0383	10
Kasauli	KSL	2.28	5.94	0.0522	2
Kashipur	KAS	1.40	6.30	0.0675	1
Keylang	KLG	12.23	1.70	0.0185	2
Khatima	KHA	1.23	13.01	0.0619	1
Kotdwar	KOT	0.60	5.21	0.0714	1
Kullu	KUL	3.00	4.17	0.0396	2
Lansdown	LAN	2.00	5.65	0.0564	1
Mandi	MAN	2.63	5.73	0.0658	3
Munsiari	MUN	1.18	4.95	0.0374	8
Nathpa	BHA	4.24	7.97	0.0474	3
Paati	PTI	7.55	2.56	0.0308	7
Palampur	PLM	3.17	5.74	0.0503	1
Pauri	PAU	2.19	5.19	0.0448	2
Pithoragarh	PTH	4.06	7.51	0.0670	11
Rampur	RAM	2.85	5.13	0.0439	2
Recong Peo	PEO	5.60	3.20	0.0532	2
Rishikesh	RIS	2.09	7.05	0.0583	1
Roorkee	ROO	1.13	5.70	0.0682	8
Rudraprayag	RUD	1.23	2.63	0.0566	2
Saluni	SAL	4.47	2.56	0.0725	1
Tanakpur	TAN	5.79	4.23	0.0519	1
Tehri	THE	2.39	4.99	0.0529	4
Tissa	TIS	9.31	2.15	0.0254	2
Una	UNA	1.63	6.23	0.0877	2
USNagar	UDH	0.99	8.04	0.0676	2
Uttarkashi	UTK	2.39	3.28	0.0525	8
Vikasnagar	VIK	2.18	10.87	0.0712	2

Anderson and Hough (1984) neglected source part (κ_s) and proposed that κ is a function of site and path terms when measured above the corner frequency (f_c). After neglecting source-term, the relation between κ and epicentral distance as proposed by Anderson and Hough (1984) is of the following form:

$$\kappa = \kappa_0 + \kappa_R \cdot R(s) \quad (4)$$

Where κ_0 is a factor accounting for attenuation due to near-surface geology.

The process of calculating κ starts with the baseline correction of records (e.g. Lai et al. 2016). After picking the P and S wave arrivals manually from the records, the five-second window of both signal, as well as background noise, is used. The background noise is selected before the P wave arrival, while the signal part is chosen after S-wave arrival. A five-second signal window consists of 0.5 seconds before S-wave arrival, while 4.5 seconds after S-wave arrival. To ensure proper data quality, the SNR is estimated in time-domain by dividing the amplitude in signal part by that of background noise and the records with sufficient SNR typically 100 are used in the data processing (e.g. Lai et al. 2016). Once the records have been analyzed in time-domain, they are transferred to the frequency domain using a fast Fourier transform algorithm for further analysis. The signal part, as well as background noise, is plotted in log-linear space to find the value of f_1 and f_2 from acceleration spectra. Konno-Ohmachi filter (Konno and Ohmachi 1998) is used to achieve the data smoothing. To double-check the quality of data only the acceleration spectra having $SNR > 3$ in frequency-domain are used in κ calculation. Since the data used to present work are acquired using high sampling frequency (200 Hz), higher values of f_2 are expected for κ calculation. However, looking at the records, a strong pulse is observed after 50 Hz, so we limit our analysis to 50 Hz only. For North-South (NS) component, the values of f_1 range from 2 to 18 Hz, while f_2 values lie between 18 and 50 Hz. In the same way, for the East-West (EW) component, f_1 values are found to range between 2 to 19 Hz and f_2 values between 17 to 50 Hz. The selected frequency range $\Delta f = f_1 - f_2$ in both components is used to estimate linear decay in spectral amplitude. The resulting κ value is determined by averaging the individual κ value obtained from both NS and EW components. Only the average κ value having little variation (less than 30%) in two components are considered. For the sites having multiple records, the κ value is estimated by averaging the κ value from the individual records. Figure 3 shows the estimated κ value for both NS and EW components at Champawat (CHP) station for an earthquake having a magnitude 5.7, recorded at an epicentral distance of 73 km. The average κ value of this record is found to be 0.0476 s.

3.1. Distance Dependence of Kappa

Many theories exist in the literature regarding the selection of distance for kappa estimation. Some researchers (Douglas et al. 2010; Ktenidou, Gélis, and Bonilla 2013) argue that the epicentral distance is a better choice, while others (Castro et al. 2000; Lai et al. 2016) claim that the hypocentral distance may be a better option. Anderson and Hough (1984), who presented the concept of kappa for the first time, used epicentral distance in their study. Since then, it has been a matter of debate, which distance should be applied. The hypocentral distance may be a better option as it is closely associated with the path followed by the seismic waves from the source to site, and reflects the regional effect on κ . However, the use of hypocentral distance includes many uncertainties like focal depth. Moreover, the main goal in kappa computation is to estimate site term in Eq. (4), which can be obtained by making $R = 0$ (κ_0). So to overcome this problem, the use of epicentral distance proposed by Anderson and Hough (1984) looks more appealing because hypocentral distance cannot equal to zero unless depth does and even if we are using crustal

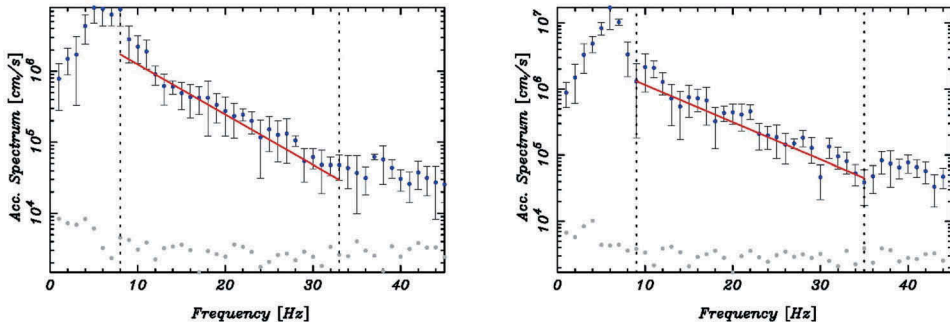
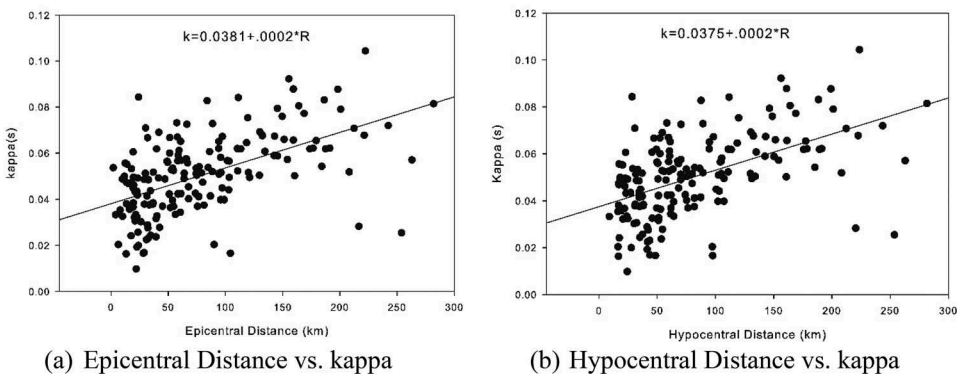


Figure 3. Kappa estimation from NS and EW component of record at Champawat (CHP) station using an earthquake having magnitude 5.7. The blue dots show the signal portion while black dots represent the noise spectrum. Using the least square estimation method κ value for NS component is 0.0518 while for the EW component, it is 0.0433.

earthquakes only. In our case, some of the used earthquakes may have depth more than 25 km, so to check the dependency of the kappa on distance, we performed regression for the whole dataset using Eq. (4). As seen from Fig. 4, very little difference is observed in the kappa value using two different distances. The kappa value using hypocentral distance is slightly lower as it includes the effect of depth as well. It looks that the distance is not going to make any accountable difference in values, but this difference may be observed closely using near source data and in the region which is more attenuative.

3.2. Relation between Kappa and Event Magnitude

As discussed previously, different researchers find the relation of κ value, with the individual source, site or path parameter, or a combination of those two or three parameters in different regions. On the same guidelines, we study the correlation of κ with all three parameters. The study of attenuation of the high-frequency decay spectrum is not possible using whole-path attenuation (Ktenidou, Gélis, and Bonilla 2013) and can be accomplished



(a) Epicentral Distance vs. kappa

(b) Hypocentral Distance vs. kappa

Figure 4. The variation of kappa with epicentral distance (a) and hypocentral distance (b). The estimated κ_0 value using epicentral distance is 0.0381 while, using hypocentral distance it is 0.0375. The κ_0 value using hypocentral distance is found slightly lower and may be due to the depth factor.

using the high-frequency band above corner frequency. The choice of corner frequency becomes a difficult task for earthquakes having a magnitude of < 3.5 . As magnitude is lowered, the corner frequency shifts towards a higher frequency side, thus allowing the smaller frequency band Δf for κ calculation. van Houtte et al. (2014) found different limits of maximum usable frequency for different magnitude earthquakes. They found if the maximum usable frequency is 40 Hz, the earthquakes having a magnitude 2.5 and above can be used reliably for κ estimation. However, for other maximum usable frequencies like 30 Hz and 23 Hz, the earthquakes of magnitude 3 and 3.5 respectively are used in the calculation. However, in our case, we are using earthquakes having a magnitude above three and SNR is high because of higher Nyquist frequency; so κ measurement is not difficult. When plotted kappa against magnitude, the κ values are found to increase linearly with magnitude, but with a significant error factor (Fig. 5). However, for lower magnitude, i.e. $M < 4$, no correlation is found between κ and magnitude. To further check the relation of κ and magnitude, we plot the minimum and maximum frequency of different earthquakes as a function of magnitude for both NS and EW components. As magnitude increases, corner frequency should be lower, thus allowing more frequency band. However, looking closely at Fig. 6, no such relationship is found between smaller frequency, higher frequency, frequency band, and magnitude. In the absence of sufficient data, we do not study the effects of other source parameters like earthquake faulting or directivity on κ concerning the observation sites.

4. Path Effect

Seismic wave attenuation plays an important role in seismic hazard analysis. As seismic waves move from source to the recording station, they get attenuated, and this attenuation can be expressed as a combination of three quantities, i.e. intrinsic attenuation, scattering attenuation, and geometric spreading. Geometrical spreading is a function of distance rather than medium properties. With the same assumption in mind, higher values of kappa should be observed at larger epicentral distances, while lower values at shorter distances. The original model of increasing kappa with distance does not necessarily apply to all studies. Sometimes owing to non-linearity (Fernández, Castro, and Huerta 2010), kappa increases to a particular distance range; after that, it becomes constant or even decreases. The difference in this kappa value may be attributed to different Q values in the upper crust (Campbell 2009). In our case, looking closely at Fig. 4, the kappa values are found to increase linearly with less scatter.

4.1. Q Value

In general, attenuation depends upon the medium through which seismic waves travel. The high-frequency ground motion attenuates faster as compared to low-frequency one (Aki and Richards 2002). The other two quantities intrinsic attenuation and scattering attenuation depend upon the medium properties and can be expressed as the inverse of a dimensionless quantity Q (representing wave amplitude decay in the medium as proposed by Knopoff 1964). Intrinsic attenuation is observed due to the conversion of seismic energy in thermal energy, and this kind of phenomenon is a function of variations in elastic properties. Scattering attenuation, on the other hand, is observed due to medium

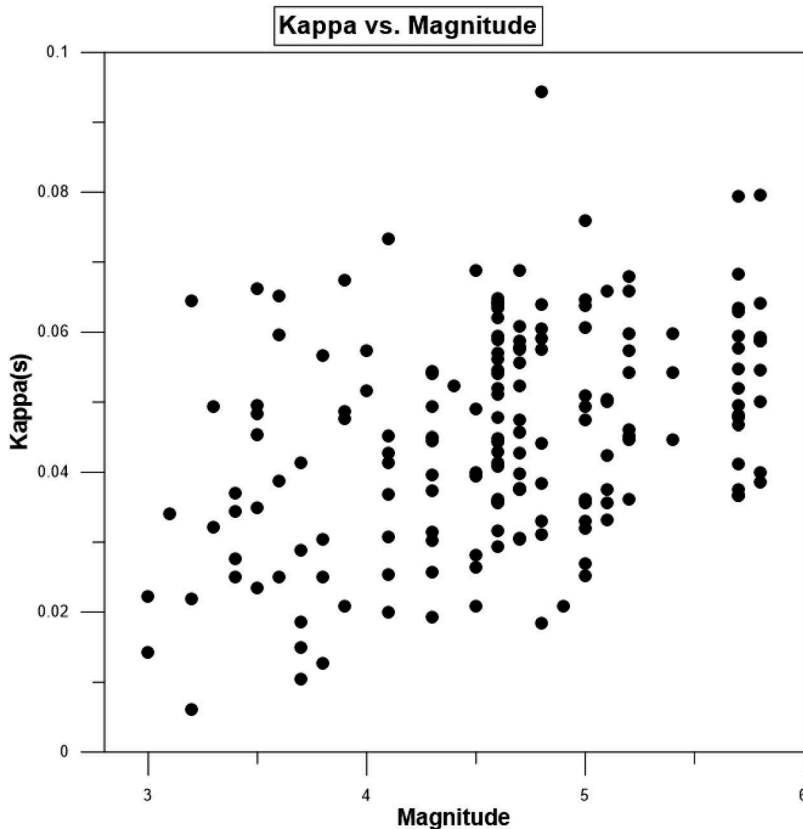


Figure 5. The variation of kappa with magnitude. Kappa values are found to increase generally with increasing magnitude for higher magnitude earthquakes (>4). For lower magnitude earthquakes (<4), a large scatter is observed in values.

heterogeneities. Q can be represented as a combination of frequency-independent intrinsic attenuation (Q_i) and frequency dependent scattering attenuation (Q_s).

In general Q value can be written as:

$$Q(f) = Q_0 f^\eta \quad (6)$$

Where Q_0 is the quality factor. Q value increases with frequency, where Q_0 represents heterogeneities in medium and η represents the seismic activity of the region. High η values in a region are an indicator of higher frequency dependency. Generally low Q_0 and higher η values are reported in seismically active regions worldwide, including the Himalayan region in India (Havskov et al. 2016; Mukhopadhyay and Sharma 2010; Sharma et al. 2008; Sharma, Mittal, and Kumar 2015; Sharma, Teotia, and Kumar 2007; Sharma et al. 2009; Singh et al. 1999). So having low Q values in a region directly relates the attenuation of ground motion either by intrinsic attenuation or scattering.

The attenuation characteristics of a region may be studied using different parts of recorded waveforms in that region. P and S waves are used to study the crustal attenuation characteristics; while coda waves are used to represent the deeper lithospheric attenuation as they are backscattered waves generated by the interaction of S waves with medium

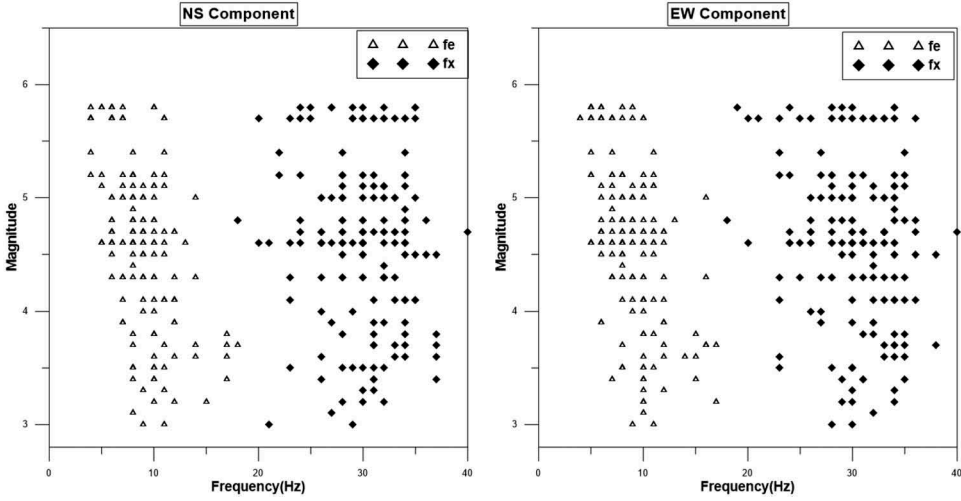


Figure 6. The relation between the minimum and maximum frequency for NS and EW components for different magnitude earthquakes. With the increase in magnitude, the usable frequency band should increase. However, looking closely at both figures, no such relation is observed.

heterogeneities. To study the relation of kappa with attenuation in the present work, the attenuation is studied using coda waves from the recorded waveforms in two regions; one in the Uttarakhand region and another in the Himachal region.

4.2. Single Backscattering Model

The single backscattering model proposed by Aki and Chouet (1975) is used to estimate Q_c values for both the regions. As mentioned earlier, in this theory, the coda waves are taken as backscattered body waves generated by the interaction of body waves with medium heterogeneities present in the Earth's crust and upper mantle. Following the same theory, scattering is supposed to be a weak process neglecting the multiple scattering, and outgoing waves are scattered only once before reaching the receiver. So, the coda amplitudes, $A_c(f, t)$ filtered at a central frequency over a narrow frequency band can be represented as a function of lapse time t , measured from the origin of a seismogram (Aki 1980).

$$A_c(f, t) = S(f)t^{-a} \exp(-\pi ft/Q_c) \quad (7)$$

where $S(f)$ represents the coda source factor at frequency f and is taken as a constant being independent of time and radiation pattern, t^{-a} represents the effect of the geometrical spreading factor for body wave, and so a is taken as 1, and Q_c is the quality factor for coda waves representing the attenuation in a medium. Taking logarithm on both sides, the above equation can be rewritten as

$$\ln(A_c(f, t)t) = \ln S(f) - (\pi f/Q_c)t \quad (8)$$

The above equation represents a straight line equation between $\ln S(f)$ and t , where $-\pi f/Q_c$ is the slope of line and $\ln S(f)$ is the intercept. Q_c can be estimated from the slope of the line and obviously for different frequency values. Plot of $\ln Q_c$ with $\ln f$ provides the

Q-f relationship. Q_c refers to the average attenuation characteristics of the region. Using long coda wave in the calculation of Q_c will reflect the attenuation characteristics of the deeper part as the time taken by the wave to traverse from earthquake source to scatterer and scatterer to recording station will increase (Pulli 1984).

4.3. Wennerberg Formulations

Various researchers have worked on studying the contribution of Q_i and Q_s in total attenuation. Wu (1985) studied these parts using the dependence of total S-wave energy on hypocentral distance. performed these studies using the energy flux model of seismic coda based on coda amplitude and decay. Wennerberg (1993) also provided a methodology to study these quantities and the theory provided by him is used here to estimate Q_i and Q_s . According to Zeng, Su, and Aki (1991), the observed value of Q_c in terms of intrinsic and scattering can be written as:

$$1/Q_c = 1/Q_i + \{1 - 2\delta(\tau)\}/Q_s \quad (9)$$

where $\delta(\tau)$ is $-1/(4.44 + 0.738\tau)$, $\tau = \omega t/Q_s$, ω is the angular frequency, and t is the lapse time, the time from the origin of an earthquake. For estimating the relative contribution of Q_i and Q_s separately, another quality factor Q_d estimated using the direct wave evaluated in the earth volume equivalent to the volume sampled by coda waves is required. Q_d can be separated into two parts according to the following equation:

$$\frac{1}{Q_d} = \frac{1}{Q_i} + \frac{1}{Q_s} \quad (10)$$

So following Wennerberg (1993), using Q_d and Q_c both quantities can be defined separately as

$$\frac{1}{Q_s} = \frac{1}{2\delta(\tau)} \left(\frac{1}{Q_d} - \frac{1}{Q_c(\tau)} \right) \quad (11)$$

$$\frac{1}{Q_i} = \frac{1}{2\delta(\tau)} \left(\frac{1}{Q_c} + \frac{2\delta(\tau) - 1}{Q_d} \right) \quad (12)$$

Q_s and Q_i can be estimated as a function of lapse time from Eqs. (9), (11) and (12), since Q_c is measured as a function of lapse time.

The Attenuation parameter, i.e. the frequency-dependent Q is estimated using two earthquake regions as shown in Fig. 2. The two regions are defined based on earthquake occurrence and separation of two regions in central Indian Himalayas. The results are estimated in terms of frequency-dependent relationship for the two regions. Figure 7 shows the original (top), filtered (left side) and the variation of $\ln(A_c(f, t)t)$ with lapse time t at various Central frequencies (right side) for one event and station pair used for estimation of Q . Frequency-dependent Coda Q_c values estimated in the Uttarakhand region (region 1) and Himachal region (region 2) are shown in Fig. 8. The plot of fitting of a straight line on average values of Q_c with respect to frequency for region 1 and 2 by which the frequency-dependent relationships are estimated are given in Fig. 9. Q_c for both, the regions are estimated keeping in mind the localized areas of central Himalaya. The average frequency-dependent relationships ($Q = Q_0 f^n$) estimated for both regions are

$Q_c = 158f^{1.18}$ and $Q_c = 194f^{1.2}$ respectively. Low values of Q_0 (< 200) and higher values of η (> 1) show that both these regions are highly heterogeneous and seismically active (Aki and Chouet 1975; Sharma et al. 2008, 2009). For separating Q_c into Q_i , and Q_s , Q_d values for the central Himalayas are taken from Sharma et al. (2009). Q_s and Q_i values range

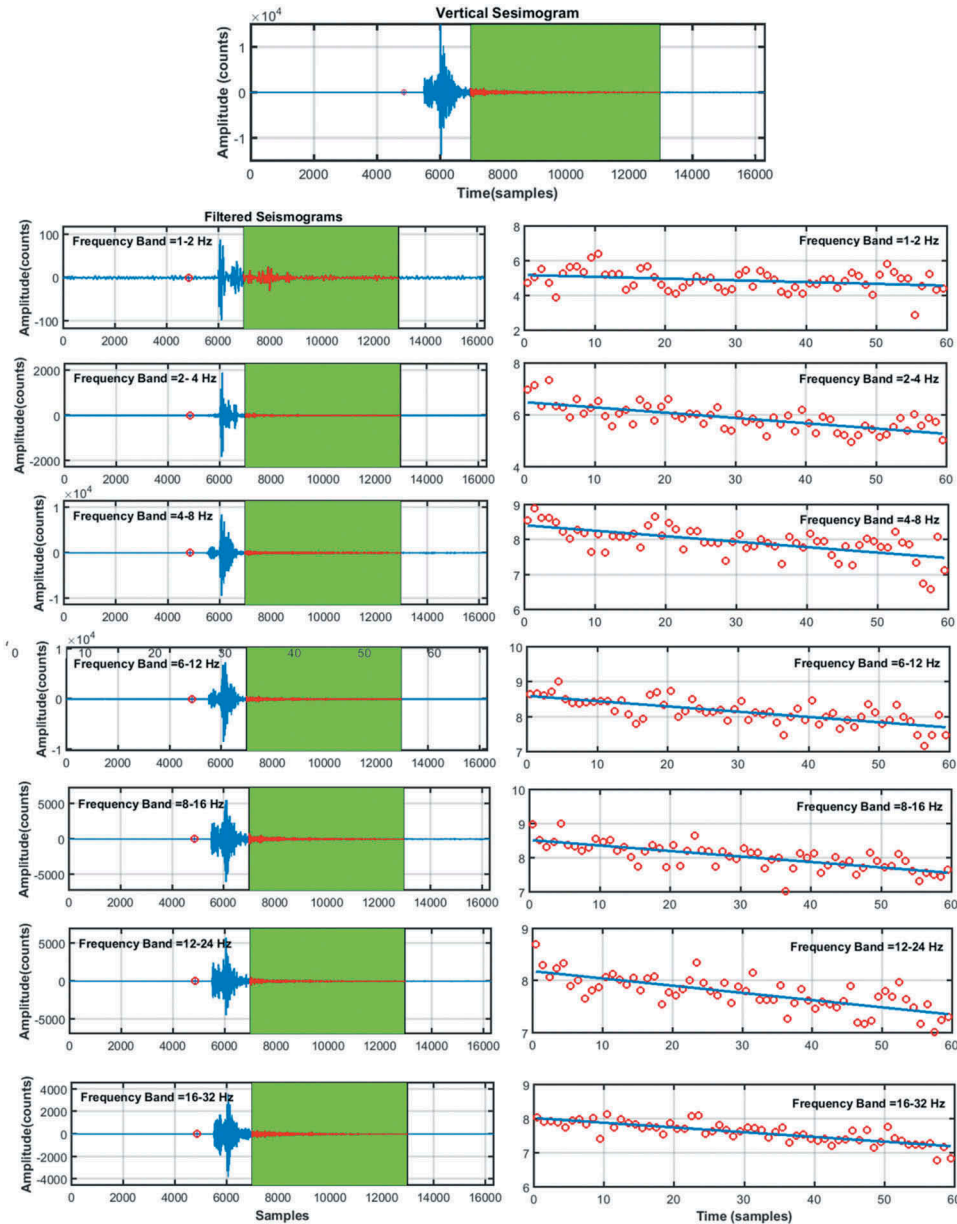


Figure 7. Original (top) and filtered seismograms (left side) at Kapkot (KAP), Uttarakhand recorded on 15/06/2015 at seven central frequencies (i.e. 1.5, 3, 6, 9, 12, 18, 24 Hz). The green shaded portion shows the coda window of 30 s or 6000 samples. The variation of $\ln(A_c(f, t))$ with lapse time t at various Central Frequencies (right side) for the same event and station pair are depicted.

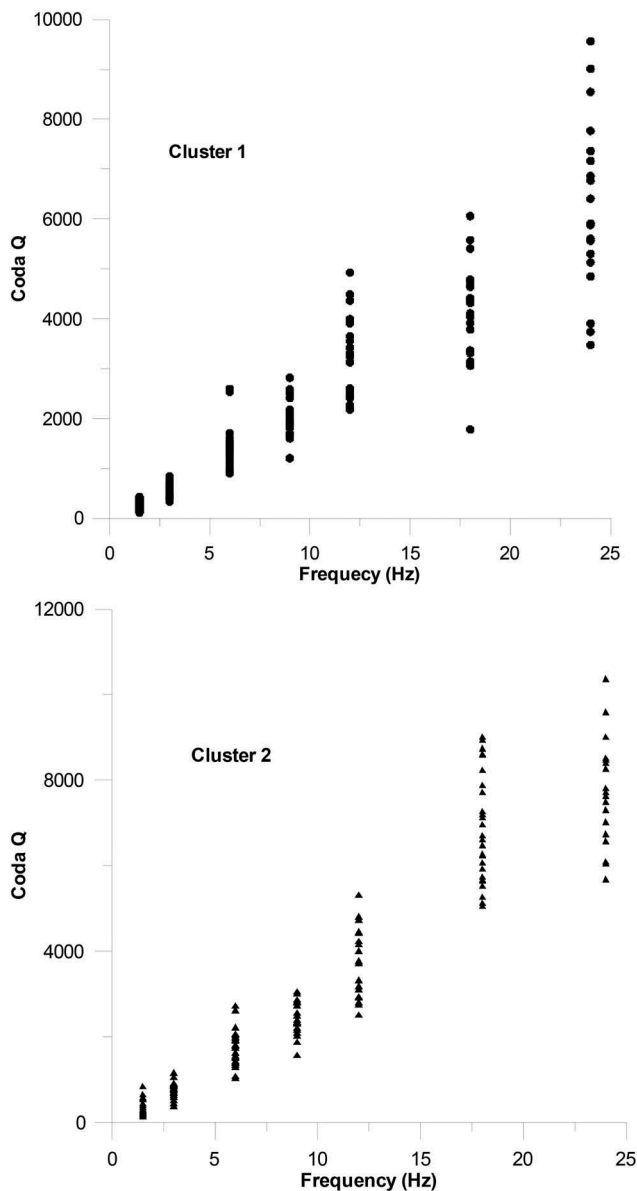


Figure 8. The estimated frequency-dependent Coda Q_c values for the Uttarakhand region (region 1) and Himachal region (region 2).

from 201 and 20 at 1.5 Hz to 2889 and 277 at 24 Hz, respectively of region 1. Similarly, for region 2, these values range between 239 and 31 at 1.5 Hz to 3122 and 302 at 24 Hz respectively. The values related to Q_c , Q_i , and Q_s for regions 1 and 2 at different frequencies are given in Tables 3 and 4 respectively. It is interesting to note that the attenuation parameters are frequency-dependent and for both the regions, intrinsic attenuation (Q_i) is more than the scattering attenuation (Q_s) for all central frequencies (Tables 3 and 4). This predominance of Q_i over Q_s predicts the behavior of the wave

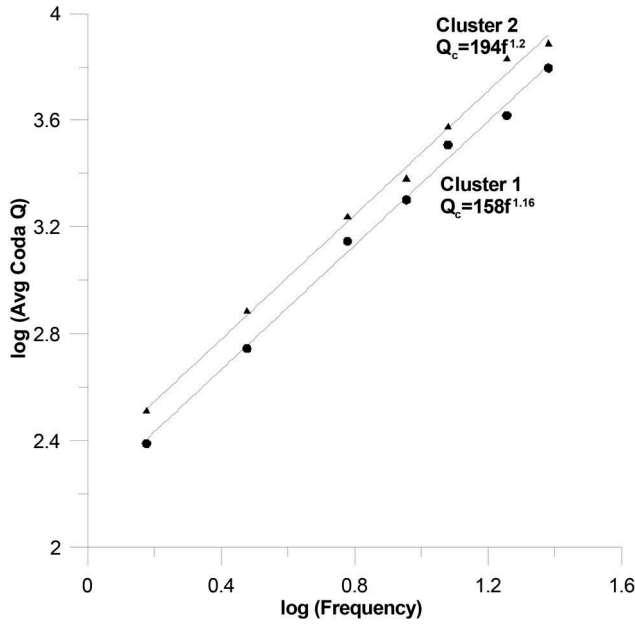


Figure 9. A plot of fit of a straight line on average values of Q_c with respect to frequency for region 1 and 2 by which the frequency-dependent relationships are estimated. Frequency-dependent relationships are also written with the corresponding line.

attenuation through the absorption within the granitic layer at shallow depths. At lower frequencies, Q_c values are found close to Q_s values, which is in agreement with the theoretical measurements suggesting the presence of complex crustal heterogeneities beneath the region affecting the propagation of seismic waves experiencing considerable decay of energy through scattering. A good review of the relation between Q and κ is provided by Campbell (2009).

5. Site Effects

The amplification or de-amplification of input ground motion at specific frequencies may be attributed to the presence of soil deposits at that site. This process is called site effects and is primarily responsible for modifying the characteristics of incoming ground motion. The importance of site effects was firstly documented long back during 1985 in

Table 3. Estimated Q_c , Q_i and Q_s values for region 1. Q_d values are taken from Sharma et al. (2009).

Frequency	Q_c _Region 1	Q_d	Q_s	Q_i
1.5	244	126	201	20
3.0	556	175	379	38
6.0	1401	299	799	75
9.0	2002	–	–	–
12.0	3217	502	1566	144
18.0	4154	–	–	–
24.0	6252	868	2889	277

Table 4. Estimated Q_c , Q_i and Q_s values for region 2. Q_d values are taken from Sharma et al. (2009).

Frequency	Q_c _Region 2	Q_d	Q_s	Q_i
1.5	323	126	239	31
3.0	766	175	448	49
6.0	1720	299	876	87
9.0	2396	–	–	–
12.0	3753	502	1664	189
18.0	6764	–	–	–
24.0	7693	868	3122	302

Mexico, where earthquakes occurring in the Gurrero gap caused severe destruction in Mexico City about 350 km away as well, along with epicentral region (Singh, Mena, and Castro 1988). Since after its recognition, site effects were generally witnessed during moderate to major earthquakes in different parts of the world. The site effects in India were also observed during some of the major earthquakes like Bhuj (January 26, 2001; M_w 7.7), as well as, Sikkim earthquake (September 18, 2011; M_w 6.9). During the Bhuj earthquake, the destruction was observed in Ahmedabad city, about 300 km away from the origin. In recent times, Nepal earthquake (April 25, 2001; M_w 7.8) caused a lot of destruction in Uttar Pradesh and Bihar regions of India, far away from the epicenter. A lot of technique has been used to estimate the site effects by various researchers (Borcherdt 1970; Lermo and Chavez-Garcia 1994; Nakamura 1989). The best method for determining site effects is based on dividing the Fourier amplitude spectra of a soil site by that of rock site, so-called reference site. This technique was originated by Borcherdt (1970) and has been used previously in various environments in India (e. g. Mittal 2011; Mittal et al. 2013; Mittal, Kumar, and Kumar 2013). The main disadvantage of this technique is the non-availability of a reference site, which may not always be available for every region. In the absence of reference sites, Nakamura (1989) proposed another technique based on dividing the Fourier amplitude spectra of the horizontal component by Fourier amplitude spectra of vertical component (HVSr). Initially, this technique was proposed for microtremors, while later on it was applied successfully to earthquake recordings (Lermo and Chavez-Garcia 1994; Mittal et al. 2015, 2016a).

HVSr technique is applied to estimate site amplification (A_{peak}), as well as predominant frequency (f_{peak}) at all the sites in central Himalaya. This technique is very reliable for estimating predominant frequency; however, the amplification determined by this technique may be misleading as the vertical component is also amplified. For estimating predominant frequency using HVSr, all the acceleration time histories are baseline corrected, and a 15 s window after shear wave arrival is chosen from all three components. Once the window has been selected, the fast Fourier transform algorithm is used to convert time series into the frequency domain. Only records having sufficient SNR in the frequency domain, typically >3 are considered in site effect estimation. Based on SNR, a minimum of three to four records at each site are found useful.

Fourier spectra of each of the three components are smoothed using a Konno and Ohmachi (1998) window with a bandwidth parameter b of 20. The average of both horizontal components is considered for estimating HVSr. The HVSr for all the earthquakes, as well as the average ratio for each site, is shown in Fig. 10.

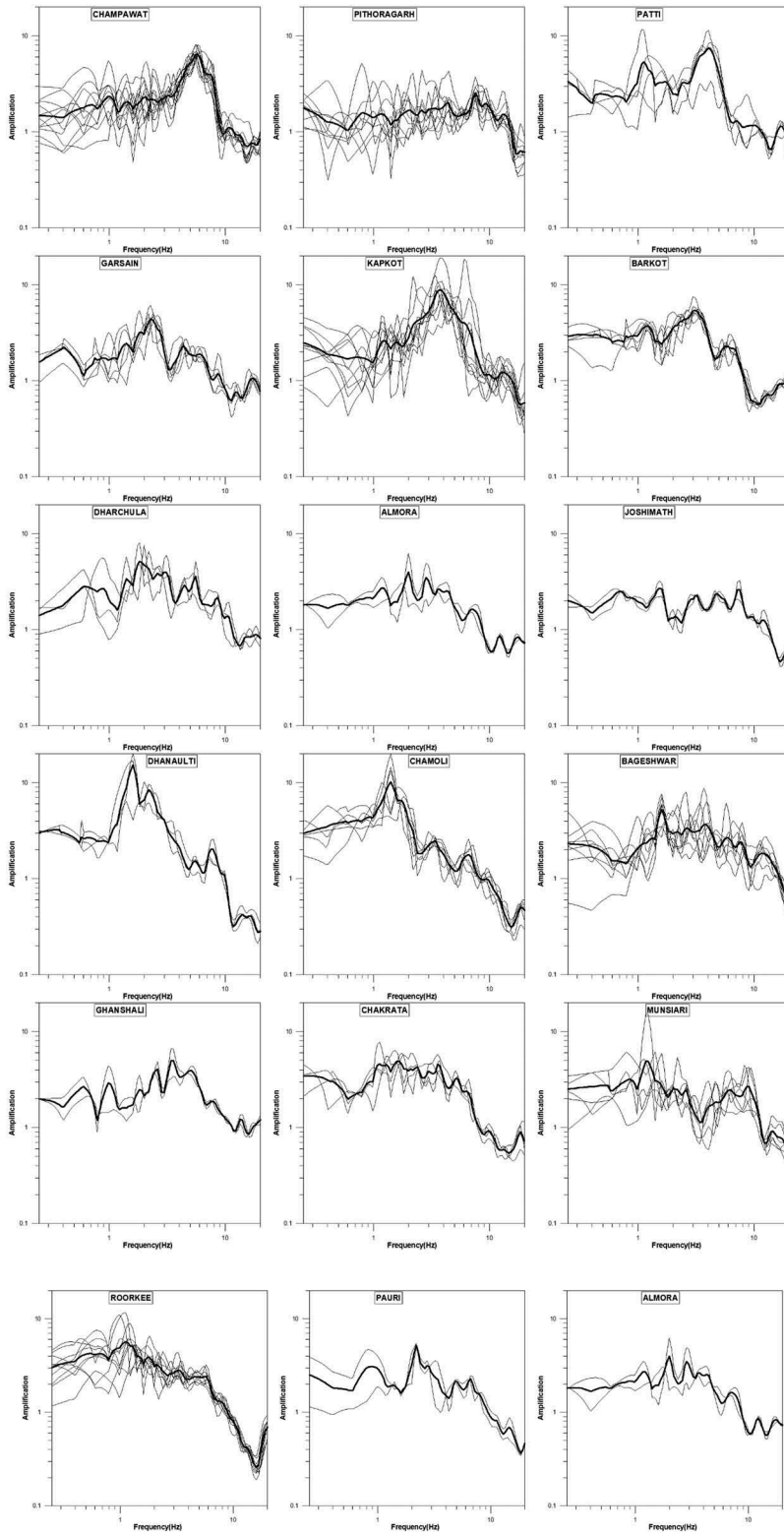


Figure 10. Amplification and predominant Frequency at some of the sites in the present study using HVSR.

Site effects play an essential role in ground motion prediction from future earthquakes and the development of GMPEs for a particular region (Douglas 2003). In earlier studies, while constructing GMPEs, only two types of sites, namely, hard rock and soft soil sites were taken into account. Later, many researchers felt that for the better estimation of ground motion or GMPE; recording sites should be further divided into different classes based on different parameters. Out of these, one of the most commonly used parameters is the time-averaged velocity in upper 30 m (V_{S30}). Various geophysical techniques including multichannel analysis of surface waves (MASW) is used to estimate V_{S30} . Nowadays, V_{S30} is the most commonly used parameter to account for site effects in different parts of the world (Boore and Atkinson 2008; Campbell and Bozorgnia 2008). However, such kind of measurements are costly and time-consuming and are not always available in every part of the world including area under study at present work. Borchardt (1994) classified sites in three different categories by combining shear wave velocity with near-surface geology. Mittal, Kumar, and Ramhmachhuani (2012) tried to organize strong-motion sites in India by modifying Borchardt (1994), but the main drawback of this site classification is that it is purely based on the geology of the area.

Here several records at different sites are used to find the HVSR curve. The recording sites in the present study can be classified into three different categories (A, B, and C) based on f_{max} . According to our results, only a few sites fall into category A (having $f_{max} > 5.5$). These sites are Champawat, Dehra, Didihat, Keylang, Paati, Tanakpur, and Tissa. Remaining sites are categorized as hard soil or soft soil sites and can be categorized as B and C based on f_{max} .

In recent times Harinarayan and Kumar (2018) categorized various strong-motion sites in the central Himalayas using extended horizontal to vertical response ratio (HVRR), which is based on dividing the 5% damping horizontal response spectra by that of vertical response spectra. They modified the classification of Mittal, Kumar, and Ramhmachhuani (2012) and allocated all central Himalaya sites broadly into four categories, namely A, B, C and D based on peak predominant frequency (f_{peak}) and amplification peak (A_{peak}). In the absence of V_{S30} or average N-SPT of 30 m (N_{30}), this scheme of characterizing sites using f_{max} looks appealing. The multiple analysis of surface waves studies are available for some of the sites of strong-motion sites in north India (Pandey et al. 2016).

The site effects should be taken care of while choosing a frequency band for κ estimation, as amplification can affect the calculations adversely. Depending upon the spectrum, κ values can vary significantly. Site amplification can hide the spectrum that should be selected for κ estimation, and sometimes it becomes difficult to choose a proper frequency band for calculation (van Houtte et al. 2014).

In general, κ is more for soil sites or stiff soil, while it is lower for hard rock sites. Site effects are supposed to be the primary factor in changing the shape of the spectra (e. g. AlShukri, Pavlis, and Vernon 1995; Fernández, Castro, and Huerta 2010; Prieto et al. 2007; Vernon et al. 1998). We also observed the same findings in our results. κ_0 value is found to be 0.0381 and 0.0375 for the epicentral distance and hypocentral distance respectively using the whole dataset. Once site classification is made based on predominant frequency, we clubbed all the rock sites and performed regression for κ_0 estimation. The estimated κ_0 value is found to be 0.0228. In a similar way, performing regression for all the soil sites gives κ_0 value 0.0389 (Fig. 11). The sites classified as class A or rock sites, experience low kappa values while sites classified as stiff soil or soil sites (class B and C, respectively) observe high kappa values (Table 2).

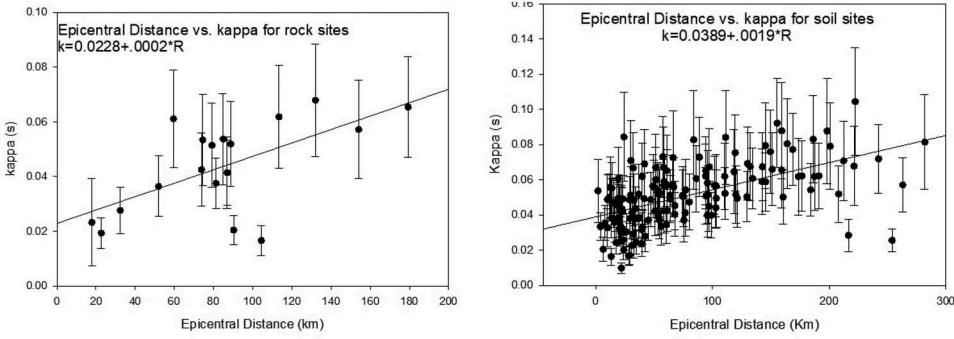


Figure 11. The variation of kappa with epicentral distance for rock sites and soil sites. The estimated κ_0 value for rock sites is 0.0228, while for soil sites it is 0.0389. The κ_0 value for rock sites is estimated using fewer points so a large scatter is observed.

6. Discussion & Conclusions

In the present work, we estimated attenuation and amplification in the central Himalayan region, with special emphasize on kappa value (κ_0) and site characteristics. Higher kappa values are reported on soil or stiff sites; whereas low values are reported at rock sites, which are in agreement with the theoretical as well as the computed attenuation parameters. Using distance dependence, no significant difference is found in κ_0 value using epicentral distance or hypocentral distance. Site effects are estimated using the HVSR approach. The predominant frequency for soil sites is found less as compared to stiff and rock sites, which is a well-known and tested phenomenon within the published literature. To testify the exposed geology, the endeavor is also made to classify sites in various classes based on predominant frequency. For all rock sites, the regression is performed for κ_0 estimation. The estimated κ_0 is 0.0228. In the same way, κ_0 for all soft sites is found to be 0.0389. To complement kappa values, the coda wave quality factor (Q_c) has been estimated for two regions in the central Himalaya region. The average frequency-dependent relationships ($Q = Q_0 f^n$) estimated for both regions are $Q_c = 158f^{1.18}$ and $Q_c = 194f^{1.2}$ respectively. The intrinsic absorption is observed to be predominant over scattering in both the regions, which shows the pattern of the subsurface to attenuate the seismic energy due to absorption within the subsurface layers. Also, the site characteristics are determined for investigating the amplification suggesting that the sites are amplified at a predominant frequency (f_{max}) between 1.5 to 10 Hz for the central Himalayan region. The attenuation and amplification parameters obtained in the present study represent a wide-ranging exploration of the propagating ground motions in the subsurface of the central Himalayan region.

7. Data and Resources

The national strong motion instrumentation network operated in India (<https://pesmos.com/>, last accessed December 15, 2018) collected the above used strong ground motion data in this work. Some of the figures used in this paper are plotted using GMT software from Wessel and Smith (1998), which is thankfully acknowledged.

Acknowledgments

The authors are thankful to the Ministry of Science and Technology (MOST) of Taiwan for funding the project, under which this study was carried out. The constructive comments from two reviewers and associate editor (Prof. Kazuhiko Kawashima) helped in improving the manuscript.

ORCID

Himanshu Mittal  <http://orcid.org/0000-0001-8836-2919>

Babita Sharma  <http://orcid.org/0000-0002-8889-0161>

Wei-an Chao  <http://orcid.org/0000-0002-3228-9107>

Yih-Min Wu  <http://orcid.org/0000-0003-4542-1741>

Ting-Li Lin  <http://orcid.org/0000-0002-7896-8092>

References

- Aki, K. 1980. Scattering and attenuation of shear waves in the lithosphere. *Journal of Geophysical Research* 85 (B11): 6496–504. doi: [10.1029/JB085iB11p06496](https://doi.org/10.1029/JB085iB11p06496).
- Aki, K., and B. Chouet. 1975. Origin of coda waves: Source, attenuation, and scattering effects. *Journal of Geophysical Research* 80 (23): 3322–42. doi: [10.1029/JB080i023p03322](https://doi.org/10.1029/JB080i023p03322).
- Aki, K., and P. G. Richards. 2002. *Quantitative seismology*. 2nd ed., 704pp University Science Books. ISBN 0-935702-96-2
- AlShukri, H. J., G. L. Pavlis, and F. L. Vernon. 1995. Site effect observations from broadband arrays. *Bulletin of the Seismological Society of America* 85 (6): 1758–69.
- Anderson, J. G., and S. E. Hough. 1984. A model for the shape of the Fourier amplitude spectrum of acceleration at high frequencies. *Bulletin of the Seismological Society of America* 74: 1969–93.
- Anderson, J. G., and J. R. Humphrey. 1991. A least squares method for objective determination of earthquake source parameters. *Seismological Research Letters* 62 (3–4): 201–09. doi: [10.1785/gssrl.62.3-4.201](https://doi.org/10.1785/gssrl.62.3-4.201).
- Biasi, G. P., and K. D. Smith (2001) Site effects for seismic monitoring stations in the vicinity of Yucca Mountain, Nevada, MOL20011204.0045, a report prepared for the US DOE/University and Community College System of Nevada (UCCSN) Cooperative Agreement.
- Boore, D. M. 2003. Simulation of ground motion using the stochastic method. *Pure and Applied Geophysics* 160 (3): 635–76. doi: [10.1007/PL00012553](https://doi.org/10.1007/PL00012553).
- Boore, D. M., and G. M. Atkinson. 2008. Ground-motion prediction equations for the average horizontal component of PGA, PGV, and 5%-damped PSA at spectral periods between 0.01 s and 10.0 s. *Earthquake Spectra* 24 (1): 99–138. doi: [10.1193/1.2830434](https://doi.org/10.1193/1.2830434).
- Borcherdt, R. D. 1970. Effects of local geology on ground motion near San Francisco Bay. *Bulletin of the Seismological Society of America* 60: 29–61.
- Borcherdt, R. D. 1994. Estimates of site-dependent response spectra for design (methodology and justification). *Earthquake Spectra* 10 (4): 617–53. doi: [10.1193/1.1585791](https://doi.org/10.1193/1.1585791).
- Bureau of Indian Standards (BIS) (2002) IS 1893 (Part 1): 2002 Indian standard criteria for earthquake resistant design of structures part 1 general provisions and buildings (fifth revision). Indian Stand.
- Campbell, K. W. 2009. Estimates of shear-wave Q and 0 for unconsolidated and semiconsolidated sediments in Eastern North America. *Bulletin of the Seismological Society of America* 99 (4): 2365–92. doi: [10.1785/0120080116](https://doi.org/10.1785/0120080116).
- Campbell, K. W., and Y. Bozorgnia. 2008. NGA ground motion model for the geometric mean horizontal component of PGA, PGV, PGD and 5% damped linear elastic response spectra for periods ranging from 0.01 to 10s. *Earthquake Spectra* 24 (1): 139–71. doi: [10.1193/1.2857546](https://doi.org/10.1193/1.2857546).

- Castro, R. R., L. Trojani, G. Monachesi, M. Mucciarelli, and M. Cattaneo. 2000. The spectral decay parameter κ in the region of Umbria-Marche, Italy. *Journal of Geophysical Research* 105 (B10): 23811–23. doi: [10.1029/2000JB900236](https://doi.org/10.1029/2000JB900236).
- Douglas, J. 2003. Earthquake ground motion estimation using strong-motion records: A review of equations for the estimation of peak ground acceleration and response spectral ordinates. *Earth-Science Reviews* 61 (1–2): 43–104. doi: [10.1016/S0012-8252\(02\)00112-5](https://doi.org/10.1016/S0012-8252(02)00112-5).
- Douglas, J., P. Gehl, L. F. Bonilla, and C. Gélis. 2010. A κ model for mainland France. *Pure and Applied Geophysics* 167 (11): 1303–15. doi: [10.1007/s00024-010-0146-5](https://doi.org/10.1007/s00024-010-0146-5).
- Fernández, A. I., R. R. Castro, and C. I. Huerta. 2010. The spectral decay parameter kappa in Northeastern Sonora, Mexico. *Bulletin of the Seismological Society of America* 100 (1): 196–206. doi: [10.1785/0120090049](https://doi.org/10.1785/0120090049).
- Gahalaut, K., and N. P. Rao. 2009. Stress field in the western Himalaya with special reference to the 8 October 2005 Muzaffarabad earthquake. *Journal of Seismology* 13 (3): 371. doi: [10.1007/s10950-008-9107-1](https://doi.org/10.1007/s10950-008-9107-1).
- Gaur, V. K., R. Chander, I. Sarkar, K. N. Khattri, and H. Sinval. 1985. Seismicity and the state of stress from investigations of local earthquakes in the Kumaon Himalaya. *Tectonophysics* 118 (3–4): 243–51. doi: [10.1016/0040-1951\(85\)90123-4](https://doi.org/10.1016/0040-1951(85)90123-4).
- Hanks, T. C. 1982. Fmax. *Bulletin of the Seismological Society of America* 72 (6A): 1867–79.
- Harinarayan, N. H., and A. Kumar. 2018. Determination of NEHRP site class of seismic recording stations in the Northwest Himalayas and its adjoining area using HVSR method. *Pure and Applied Geophysics* 175 (1): 89–107. doi: [10.1007/s00024-017-1696-6](https://doi.org/10.1007/s00024-017-1696-6).
- Havskov, J., M. B. Sørensen, D. Vales, M. Özyazıcıoğlu, G. Sánchez, and B. Li. 2016. Coda Q in different tectonic areas, influence of processing parameters. *Bulletin of the Seismological Society of America* 106 (3): 956–70. doi: [10.1785/0120150359](https://doi.org/10.1785/0120150359).
- Hough, S. E., and J. G. Anderson. 1988. High-frequency spectra observed at Anza, California: Implications for Q structure. *Bulletin of the Seismological Society of America* 78 (2): 692–707.
- Khattri, K. N. 1987. Great earthquakes, seismicity gaps and potential for earthquake disaster along the Himalaya plate boundary. *Tectonophysics* 138 (1): 92–99. doi: [10.1016/0040-1951\(87\)90067-9](https://doi.org/10.1016/0040-1951(87)90067-9).
- Khattri, K. N. 1999. Probabilities of occurrence of great earthquakes in the Himalaya. *Proceedings of the Indian Academy of Sciences-Earth and Planetary Sciences* 108 (2): 87–92.
- Khattri, K. N., R. Chander, V. K. Gaur, and I. Sarkar. 1989. New seismological results on the tectonics of the Garhwal Himalaya. *Proceedings of the Indian Academy of Sciences-Earth and Planetary Sciences* 98 (1): 91–109. doi: [10.1007/BF02880378](https://doi.org/10.1007/BF02880378).
- Knopoff, L. 1964. *Quality Reviews of Geophysics* 2 (4): 625–60. doi: [10.1029/RG002i004p00625](https://doi.org/10.1029/RG002i004p00625).
- Konno, K., and T. Ohmachi. 1998. Ground-motion characteristics estimated from spectral ratio between horizontal and vertical components of microtremor. *Bulletin of the Seismological Society of America* 88: 228–41.
- Ktenidou, O.-J., C. Gélis, and L.-F. Bonilla. 2013. A study on the variability of Kappa (κ) in a borehole: implications of the computation process. *Bulletin of the Seismological Society of America* 103 (2A): 1048–68. doi: [10.1785/0120120093](https://doi.org/10.1785/0120120093).
- Ktenidou, O.-J., W. J. Silva, R. B. Darragh, N. A. Abrahamson, and T. Kishida. 2017. Squeezing Kappa (κ) out of the transportable array: A strategy for using bandlimited data in regions of sparse seismicity. *Bulletin of the Seismological Society of America* 107 (1): 256–75. doi: [10.1785/0120150301](https://doi.org/10.1785/0120150301).
- Kumar, A., A. Kumar, and H. Mittal. 2013. Earthquake source parameters review in Indian context. *Research and Development (IJCSEIERD)* 3 (1): 41–52.
- Kumar, A., and H. Mittal. 2018. Strong-motion instrumentation: Current status and future scenario. In *Advances in Indian earthquake engineering and seismology*, ed. M. Sharma, M. Shrikhande, and H. Wason, 35–54. Cham: Springer. doi:[10.1007/978-3-319-76855-7_3](https://doi.org/10.1007/978-3-319-76855-7_3).
- Kumar, A., H. Mittal, R. Kumar, and R. S. Ahluwalia. 2017. Empirical attenuation relationship for peak ground horizontal acceleration for North-East Himalaya. *Vietnam Journal of Earth Sciences* 39 (1): 46–56.
- Kumar, D., V. S. Ram, and K. N. Khattri. 2006. A study of source parameters, site amplification functions and average effective shear wave quality factor Q_{seff} from analysis of accelerograms of

- the 1999 Chamoli earthquake, Himalaya. *Pure and Applied Geophysics* 163 (7): 1369–98. doi: [10.1007/s00024-006-0078-2](https://doi.org/10.1007/s00024-006-0078-2).
- Lai, T.-S., H. Mittal, W.-A. Chao, and Y.-M. Wu. 2016. A study on Kappa value in Taiwan using borehole and surface seismic array. *Bulletin of the Seismological Society of America* 106 (4): 1509–17. doi: [10.1785/0120160004](https://doi.org/10.1785/0120160004).
- Lermo, J., and F. J. Chavez-Garcia. 1994. Are microtremors useful in site response evaluation? *Bulletin of the Seismological Society of America* 84: 1350–64. doi: [10.1306/080700710318](https://doi.org/10.1306/080700710318).
- Mena, B., P. M. Mai, K. B. Olsen, M. D. Purvance, and J. N. Brune. 2010. Hybrid broadband ground-motion simulation using scattering green's functions: Application to large-magnitude events. *Bulletin of the Seismological Society of America* 100 (5A): 2143–62. doi: [10.1785/0120080318](https://doi.org/10.1785/0120080318).
- Mittal, H. (2011) Estimation of ground motion in Delhi. Ph.D. thesis, Dept. of Earthquake Engineering, Indian Institute of Technology, Roorkee, India.
- Mittal, H., S. Gupta, A. Srivastava, R. N. Dubey, and A. Kumar (2006) National strong motion instrumentation project: An overview. In 13th Symposium on Earthquake Engineering, Indian Institute of Technology, Roorkee, Dec 18–20, 107–15.
- Mittal, H., Kamal, A. Kumar, and S. K. Singh. 2013. Estimation of site effects in Delhi using standard spectral ratio. *Soil Dynamics and Earthquake Engineering* 50: 53–61. doi: [10.1016/j.soildyn.2013.03.004](https://doi.org/10.1016/j.soildyn.2013.03.004).
- Mittal, H., and A. Kumar. 2015. Stochastic finite-fault modeling of M w 5.4 earthquake along Uttarakhand–Nepal border. *Natural Hazards* 75 (2): 1145–66. doi: [10.1007/s11069-014-1367-1](https://doi.org/10.1007/s11069-014-1367-1).
- Mittal, H., A. Kumar, and Kamal. 2013. Ground motion estimation in Delhi from postulated regional and local earthquakes. *Journal of Seismology* 17 (2): 593–605. doi: [10.1007/s10950-012-9340-5](https://doi.org/10.1007/s10950-012-9340-5).
- Mittal, H., A. Kumar, and A. Kumar. 2013. Site effects estimation in Delhi from the Indian strong motion instrumentation network. *Seismological Research Letters* 84 (1): 33–41. doi: [10.1785/0220120058](https://doi.org/10.1785/0220120058).
- Mittal, H., A. Kumar, A. Kumar, and R. Kumar. 2015. Analysis of ground motion in Delhi from earthquakes recorded by strong motion network. *Arabian Journal of Geosciences* 8 (4): 2005–17. doi: [10.1007/s12517-014-1357-3](https://doi.org/10.1007/s12517-014-1357-3).
- Mittal, H., A. Kumar, and R. Ramhmachhuani. 2012. Indian national strong motion instrumentation network and site characterization of its stations. *International Journal of Geosciences* 3 (6): 1151–67. doi: [10.4236/ijg.2012.326117](https://doi.org/10.4236/ijg.2012.326117).
- Mittal, H., A. Kumar, Y.-M. Wu, K. Kumar, and A. Kumar. 2016a. Source study of M w 5.4 April 4, 2011 India–Nepal border earthquake and scenario events in the Kumaon–Garhwal Region. *Arabian Journal of Geosciences* 9 (5): 348. doi: [10.1007/s12517-016-2330-0](https://doi.org/10.1007/s12517-016-2330-0).
- Mittal, H., Y.-M. Wu, D.-Y. Chen, and W.-A. Chao. 2016b. Stochastic finite modeling of ground motion for March 5, 2012, Mw 4.6 earthquake and scenario greater magnitude earthquake in the proximity of Delhi. *Natural Hazards* 82 (2): 1123–46. doi: [10.1007/s11069-016-2236-x](https://doi.org/10.1007/s11069-016-2236-x).
- Mittal, H., Y.-M. Wu, T.-L. Lin, C. P. Legendre, S. Gupta, and B. M. Yang. 2019a. Time-dependent shake map for Uttarakhand Himalayas, India, using recorded earthquakes. *Acta Geophysica* 67 (3): 753–63. doi: [10.1007/s11600-019-00281-7](https://doi.org/10.1007/s11600-019-00281-7).
- Mittal, H., Y. M. Wu, M. L. Sharma, T. L. Lin, and B. M. Yang (2018) Shake maps generation for Delhi region using two different algorithms. In 16th symposium on earthquake engineering, Indian Institute of Technology, Roorkee, Dec 20–22, 1–10.
- Mittal, H., Y.-M. Wu, M. L. Sharma, B. M. Yang, and S. Gupta. 2019b. Testing the performance of earthquake early warning system in northern India. *Acta Geophysica* 67 (1): 59–75. doi: [10.1007/s11600-018-0210-6](https://doi.org/10.1007/s11600-018-0210-6).
- Motazedian, D., and G. M. Atkinson. 2005. Stochastic finite-fault modeling based on a dynamic corner frequency. *Bulletin of the Seismological Society of America* 95 (3): 995–1010. doi: [10.1785/0120030207](https://doi.org/10.1785/0120030207).
- Mukhopadhyay, S., and J. Sharma. 2010. Attenuation characteristics of Garhwal–Kumaun Himalayas from analysis of coda of local earthquakes. *Journal of Seismology* 14 (4): 693–713. doi: [10.1007/s10950-010-9192-9](https://doi.org/10.1007/s10950-010-9192-9).

- Nakamura, Y. 1989. A method for dynamic characteristics estimation of subsurface using micro-tremor on the ground surface. Railway technical research institute. *Quarterly Reports* 30 (1): 25–33.
- Nath, S. K., K. Shukla, and M. Vyas. 2008. Seismic hazard scenario and attenuation model of the Garhwal Himalaya using near-field synthesis from weak motion seismometry. *Journal of Earth System Science* 117 (S2): 649–70. doi: [10.1007/s12040-008-0062-6](https://doi.org/10.1007/s12040-008-0062-6).
- Pandey, B., R. S. Jakka, A. Kumar, and H. Mittal. 2016. Site characterization of strong-motion recording stations of delhi using joint inversion of phase velocity dispersion and H/V curve. *Bulletin of the Seismological Society of America* 106 (3): 1254–66. doi: [10.1785/0120150135](https://doi.org/10.1785/0120150135).
- Papageorgiou, A. S., and K. Aki. 1983. A specific barrier model for the quantitative description of inhomogeneous faulting and the prediction of strong ground motion. I. Description of the model. *Bulletin of the Seismological Society of America* 73 (3): 693–722. doi: [10.1016/0148-9062\(84\)90498-4](https://doi.org/10.1016/0148-9062(84)90498-4).
- Perron, V., F. Hollender, P.-Y. Bard, C. Gélis, C. Guyonnet-Benaize, B. Hernandez, and O.-J. Ktenidou. 2017. Robustness of kappa (κ) measurement in low-to-moderate seismicity areas: Insight from a site-specific study in Provence, France. *Bulletin of the Seismological Society of America* 107 (5): 2272–92. doi: [10.1785/0120160374](https://doi.org/10.1785/0120160374).
- Prieto, G. A., D. J. Thomson, F. L. Vernon, P. M. Shearer, and R. L. Parker. 2007. Confidence intervals for earthquake source parameters. *Geophysical Journal International* 168 (3): 1227–34. doi: [10.1111/j.1365-246X.2006.03257.x](https://doi.org/10.1111/j.1365-246X.2006.03257.x).
- Pulli, J. 1984. Attenuation of Coda waves in New England. *Bulletin of the Seismological Society of America* 74 (4): 1149–66.
- Purvanca, M. D., and J. G. Anderson. 2003. A comprehensive study of the observed spectral decay in strong-motion accelerations recorded in Guerrero, Mexico. *Bulletin of the Seismological Society of America* 93 (2): 600–11. doi: [10.1785/0120020065](https://doi.org/10.1785/0120020065).
- Seeber, L., and J. G. Armbruster. 1981. Great detachment earthquakes along the Himalayan arc and long-term forecasting. *Earthquake Prediction: An International Review* 4: 259–77.
- Sharma, B., A. K. Gupta, D. K. Devi, D. Kumar, S. S. Teotia, and B. K. Rastogi. 2008. Attenuation of high-frequency seismic waves in Kachchh Region, Gujarat, India. *Bulletin of the Seismological Society of America* 98 (5): 2325–40. doi: [10.1785/0120070224](https://doi.org/10.1785/0120070224).
- Sharma, B., H. Mittal, and A. Kumar. 2015. A reappraisal of attenuation of seismic waves and its relevance towards seismic hazard. *International Journal of Advanced Research* 3 (3): 296–305.
- Sharma, B., S. S. Teotia, and D. Kumar. 2007. Attenuation of P, S, and coda waves in Koyna region, India. *Journal of Seismology* 11 (3): 327–44. doi: [10.1007/s10950-007-9057-z](https://doi.org/10.1007/s10950-007-9057-z).
- Sharma, B., S. S. Teotia, D. Kumar, and P. S. Raju. 2009. Attenuation of P- and S-waves in the Chamoli Region, Himalaya, India. *Pure and Applied Geophysics* 166 (12): 1949. doi: [10.1007/s00024-009-0527-9](https://doi.org/10.1007/s00024-009-0527-9).
- Sharma, J., S. Chopra, and K. S. Roy. 2014. Estimation of source parameters, quality factor (Qs), and site characteristics using accelerograms: Uttarakhand Himalaya region. *Bulletin of the Seismological Society of America* 104 (1): 360–80. doi: [10.1785/0120120304](https://doi.org/10.1785/0120120304).
- Silva, W. J., and R. B. Darragh (1995) Engineering characterization of strong ground motion recorded flat rock sites. CA. Report No. TR-102262, Electric Power Research Institute, Palo Alto.
- Singh, S. K. W. K. Mohanty, B. K. Bansal, and G. S. Roonwal. 2002. Ground motion in Delhi from future large/great earthquakes in the central seismic gap of the Himalayan Arc. *Bulletin of the Seismological Society of America* 92 (2): 555–69. doi: [10.1785/0120010139](https://doi.org/10.1785/0120010139).
- Singh, S. K., E. Mena, and R. Castro. 1988. Some aspects of source characteristics of the 19 September 1985 Michoacan earthquake and ground motion amplification in and near Mexico City from strong-motion data. *Bulletin of the Seismological Society of America* 78 (2): 451–77. doi: [10.1017/CBO9781107415324.004](https://doi.org/10.1017/CBO9781107415324.004).
- Singh, S. K., M. Ordaz, R. S. Dattatrayam, and H. K. Gupta. 1999. A spectral analysis of the 21 May 1997, Jabalpur, India, earthquake (Mw = 5.8) and estimation of ground motion from future earthquakes in the Indian shield region. *Bulletin of the Seismological Society of America* 89 (6): 1620–30.

- Tsai, C.-C. P., and K.C. Chen. 2000. A model for the high-cut process of strong-motion accelerations in terms of distance, magnitude, and site condition: An example from the smart 1 array, Lotung, Taiwan. *Bulletin of the Seismological Society of America* 90 (6): 1535–42. doi: [10.1785/0120000010](https://doi.org/10.1785/0120000010).
- van Houtte, C., O.-J. Ktenidou, T. Larkin, and C. Holden. 2014. Hard-site 0 (Kappa) calculations for Christchurch, New Zealand, and comparison with local ground-motion prediction models. *Bulletin of the Seismological Society of America* 104 (4): 1899–913. doi: [10.1785/0120130271](https://doi.org/10.1785/0120130271).
- Vernon, F. L., G. L. Pavlis, T. J. Owens, D. E. McNamara, and P. N. Anderson. 1998. Near-surface scattering effects observed with a high-frequency phased array at Pinyon Flats, California. *Bulletin of the Seismological Society of America* 88 (6): 1548–60.
- Wennerberg, L. 1993. Multiple-scattering interpretations of coda-Q measurements. *Bulletin of the Seismological Society of America* 83 (1): 279–90. doi: [10.1144/GSL.SP.1996.001.01.12](https://doi.org/10.1144/GSL.SP.1996.001.01.12).
- Wessel, P., and W. H. F. Smith. 1998. New, improved version of generic mapping tools released. *Eos. Eos, Transactions American Geophysical Union* 79 (47): 579. doi: [10.1029/98EO00426](https://doi.org/10.1029/98EO00426).
- Wu, R.-S. 1985. Multiple scattering and energy transfer of seismic waves – Separation of scattering effect from intrinsic attenuation – I. Theoretical modelling. *Geophysical Journal International* 82 (1): 57–80. doi: [10.1111/j.1365-246X.1985.tb05128.x](https://doi.org/10.1111/j.1365-246X.1985.tb05128.x).
- Zeng, Y., F. Su, and K. Aki. 1991. Scattering wave energy propagation in a random isotropic scattering medium: 1. Theory. *Journal of Geophysical Research* 96 (B1): 607–19. doi: [10.1029/90JB02012](https://doi.org/10.1029/90JB02012).